



**VICTORIA UNIVERSITY**  
MELBOURNE AUSTRALIA

## *Optimized Interference Canceling for Colocated Base Station Transceivers*

This is the Accepted version of the following publication

Ahmed, Shabbir and Faulkner, Michael (2011) Optimized Interference Canceling for Colocated Base Station Transceivers. IEEE Transactions on Vehicular Technology, 60 (9). pp. 4175-4183. ISSN 0018-9545

The publisher's official version can be found at  
[http://ieeexplore.ieee.org/xpls/abs\\_all.jsp?arnumber=6036192](http://ieeexplore.ieee.org/xpls/abs_all.jsp?arnumber=6036192)  
Note that access to this version may require subscription.

Downloaded from VU Research Repository <https://vuir.vu.edu.au/9203/>

# Optimized Interference Canceling for Co-located Base Station Transceivers

Shabbir Ahmed, *Student Member, IEEE*, and Mike Faulkner, *Member, IEEE*

**Abstract**—Strong jamming signals from co-located transmitters can cause intermodulation and desensitization in receiver circuits. Cancellation circuits can remove the interference, but generate noise and distortion of their own. We analyze such a system using a Signal to Interference and Noise Ratio measure. We show that the cancellation coupler can be optimized to maximizes the Signal to Interference and Noise Ratio. The optimum coupler value is proportional to the expected level of the jammers. A hardware prototype reduced the jammers by 46dB in a controlled experiment and by 25dB in an over-the-air experiment. A convergence time of 8.4ms was sufficient for this application.

**Index Terms**—Co-location, Intermodulation distortion, Interference suppression, Land mobile radio equipment, Radio receivers.

## I. INTRODUCTION

CO-LOCATION of multi-platform transceivers on one common site has been a major challenge for radio frequency (RF) systems in different fields of communication. Government armed forces with many different platforms are often forced to share a small site because of their mobile nature (e.g. battleships, aircrafts, and vehicles) [1] [2]. RF platforms range from VHF/UHF dual-band multi-mode for voice and digital communications, UHF satellite communications transceiver, UHF transceiver for line-of-sight tactical communications, GPS receivers, radars, surveillance systems, and others. They all have the potential to interfere with each other because of the close proximity of the antennas. In recent times co-location has been an area of concern for many commercial wireless service providers. Service providers are having to deploy a larger number of base stations every year to provide for the fast growing subscriber base. In addition to this there is a growing trend for base station consolidation amongst different service providers. Here many service providers share the same site and this reduces maintenance, rental, logistics and other costs. Also community concerns such as visual pollution and health are making it difficult to establish new green field base station sites.

Co-location of base stations helps in reducing the near far problem at the user equipments (UE) because both desired and unwanted signals have a similar signal strength. This allows UEs to have reduced filtering and dynamic range requirements. But, co-location is a major disadvantage for the base station receivers themselves; they have to receive weak desired signals in the presence of high power transmit signals from neighboring base station antennas. The spectrum can

get congested very quickly because each additional antenna can carry many transmissions at different carrier frequencies. Multi-carrier power amplifiers or multi-coupling networks of cavity filters are often used to combine the high power signals prior to the antenna. At the victim receiver, such high power transmit/jamming signals cause desensitization and blocking [3] [4] by forcing its circuits into saturation. A more significant concern is the formation of intermodulation products.

The low noise amplifier (LNA) and mixer stages are most susceptible to large jamming signals. Odd order and especially third-order intermodulation products (IM3) are generated and cause spectral expansion of the jamming signal into its adjacent channels, which decays with frequency. If more than one high power jammer exists then intermodulation spurs are generated at multiples of the carrier separation. These can fall on the receive channel. Even order products are caused by circuit imbalances or self-mixing in the mixer. In the case of a direct conversion receiver, the second-order intermodulation products fall directly on the baseband irrespective of the jammer's frequency [5].

One of the issues of co-location is that the early occupier of the site initially experiences none of these problems. As more transmitters are added, sensitivity degrades. A possible solution is to replace the victim transceiver with one that has a higher dynamic range. However, this is expensive and the initial occupier would be very reluctant to pay. Therefore, there is a need for some method that can mitigate the problem without requiring a modification or any intrusion into the existing transceiver hardware. A potential solution is to reduce the powers of the jamming signals as seen by the victim receiver.

Netcom [6] proposed a non-intrusive solution that involved the placement of band pass filters in front of the LNA to admit only the desired signals. However, complex and expensive high Q cavity filters with low insertion loss would be required to sufficiently attenuate the large transmitter signals, which, in some cases, have output powers of +47dBm (50W) [7]. The problem is more difficult if the filters have to be tunable.

Authors of [1] have used computer simulations to model the co-location scenario and predict the characteristics of the jamming signals. This requires knowledge of the co-located transceiver specifications and antenna configurations. A fixed customized filter is then deployed to mitigate the interference. Unfortunately, many co-site scenarios require a certain level of adaption to handle changing carrier frequencies and ON/OFF keying of transmitters. The approach described in [2] located the jamming signal by scanning the spectrum with a Fast Fourier Transform (FFT) and then removed it with a tunable notch filter. The filter complexity issues however remain.

The authors are with the College of Engineering and Science, Victoria University, PO Box 14428, Melbourne, Victoria 8001, Australia (email: Shabbir.Ahmed@live.vu.edu.au, Mike.Faulkner@vu.edu.au).

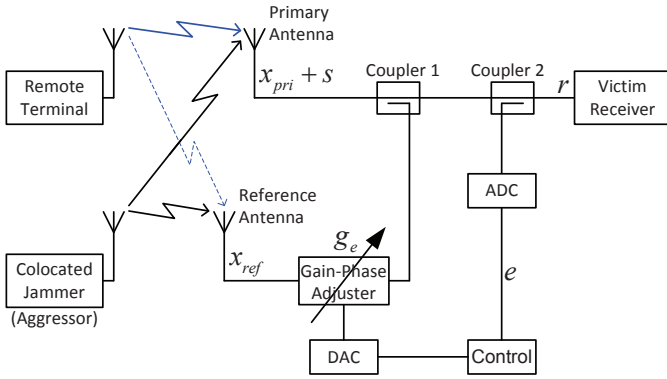


Fig. 1. An Adaptive Cancellation System

UE devices operating in frequency division duplex (FDD) also have the problem of the transmitter acting as an aggressor on to the receiver. The regular solution is to use passive SAW (surface acoustic wave) duplexing filters, but their power handling is not high enough when used in base station environments. An alternate approach taken by authors of [8] and [9] is to use cancellation loops. A direct feed from the transmitter is used in an adaptive feed-forward cancellation loop to effectively remove the interfering transmit signal and noise from the receiver. Both papers publish good cancellation performance, however neither of them consider noise and distortion generated in the canceling loops themselves. This is a key factor in any practical deployment, particularly when power levels are high.

In a co-located base station scenario each of the transceivers are independent and a direct feed from co-located aggressor transmitters is not always possible. In this paper we consider a related canceling technique that is similar to adaptive noise cancellation [10]. Our paper describes an adaptive cancellation system that is capable of mitigating interference from one such co-located antenna, as depicted in Fig. 1. The primary antenna picks up the desired signal ( $s$ ) with the jamming signal ( $x_{pri}$ ). The reference antenna is directed to pick only the jamming signal ( $x_{ref}$ ) (or more practically have a much larger interference to signal ratio than the primary). The reference input is then gain and phase adjusted and coupled into the primary path to cancel the jamming signal.

The cancellation system in mitigating large co-located jammers effectively increases the receivers capacity to handle strong signals. However, the effective distortion and noise of the total system now depends on the characteristic properties of the gain-phase adjuster (GPA) in the reference path. Ideally the GPA should not produce any distortions or noise, but in reality that is not possible. Hence, the goal is to limit the distortion and the noise generated by the reference path to a level that is lower than the distortion and noise generated by the receiver on its own without the cancellation system.

As in most RF circuits it is possible to trade off noise for distortion and vice-a-versa. In this system it is *Coupler 1* that determines the trade-off [11]. If the coupling is weak then a larger canceling signal,  $x_{ref}$ , is needed to remove  $x_{pri}$ , which toughens the IP3 (third order intercept point) requirements for the canceling branch. On the other hand a strong coupling

coefficient reduces the desired signal,  $s$ , and contributes to an increase in the receiver noise figure. The cancellation coupler is therefore a compromise between achieving higher values of IP3 and lower values of noise figure. To our knowledge no analysis has shown what the optimum coupling should be.

In this paper we carry out a novel signal to interference and noise ratio (SINR) analysis on the cancellation system. We develop an expression for the optimum coupler value that maximizes the SINR. In addition we describe an automated cancellation system that studies the energy at the output of the cancellation using an Universal Software Radio Peripheral (USRP) [12] and minimizes the energy using an one dimensional iterative search algorithm. We then carry out experiments to show that our theoretical analysis aligns with practical results. A significant improvement in SINR can be achieved using this cancellation system. Further, an over-the-air setup illustrates the effects of the system on the wanted signal.

Section II derives theoretical expressions for the SINR of the system and then Section III derives an equation for the optimum coupler. Section IV describes the hardware setup and convergence technique of the cancellation system. Section V compares SINR results from the test-bed with the theoretical predictions. Section VI addresses practical issues of the over-the-air deployment. And finally Section VII is the conclusion.

## II. DERIVATION OF SIGNAL TO INTERFERENCE AND NOISE RATIO (SINR) FOR THE CANCELLATION SYSTEM

The compromise between the level of intermodulation distortion and noise at the receiver can be evaluated simultaneously with a single parameter, i.e. the SINR. In this section we develop expressions for the desired signal, noise and third-order intermodulation distortion from which the SINR can be evaluated.

In this paper it is to be noted that lower case variables represent complex envelop voltages that characterizes both the amplitude and the gain of the signal, and upper case variables represent respective powers, e.g.  $S = \frac{E\{|s|^2\}}{2}$ . In order to analyze the circuit, the proposed system in Fig. 1 is redrawn with *Coupler 1* and *Coupler 2* restructured as shown in Fig. 2. The sampling *Coupler 2* extracts the feedback signal for the convergence algorithm. The signal of interest for the feedback circuit is the residue of the canceled jamming signal,  $X_3$ . This signal is not required to be totally eliminated provided it is reduced to a level that produces no significant intermodulation in the receiver. As such the feedback signal is still large and so there is no undesirable consequences if it is further attenuated through *Coupler 2*. In fact it is desirable to have a weak coupling value so that the sensitivity of the receiver to the wanted signal,  $S$ , is least effected. Here we assume a coupling value of  $\leq -20\text{dB}$ , such that it has negligible through path loss (ie.  $G_{CPL2} \approx 1$ ).

*Coupler 1* cancels the jammer. The coupling path gain is  $C$  and hence the through path gain is  $1 - C$ . We note that the domain of  $C$  is limited to  $0 < C < 1$ . Couplers are passive devices and are assumed not to produce any distortion.

Fig. 2 illustrates the IP3,  $IIP3_{RX}$ , and the noise temperature,  $T_{RX}$ , of the receiver referred to its input. The gain

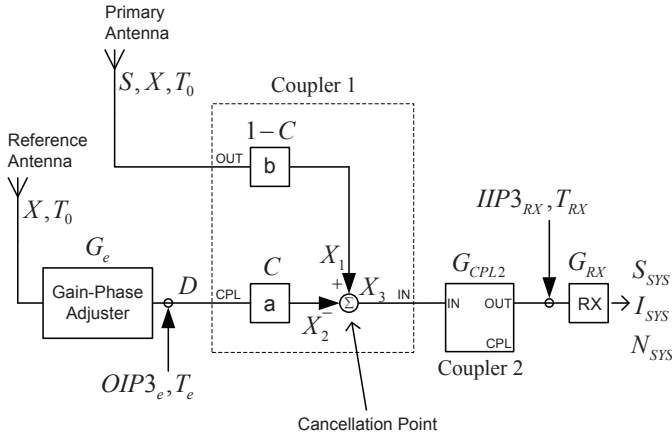


Fig. 2. Signal to Interference Noise Analysis

of the receiver is  $G_{RX}$ . However, the output IP3,  $OIP3_e$ , and the noise temperature,  $T_e$ , of the GPA is specified at its output, to be compatible with data sheet specifications of some devices, as well as to isolate the system optimization from the components in the reference path. Note, the effective  $G_e$ ,  $OIP3_e$  and  $T_e$  of the reference arm is often the combination of a number of components including attenuators, amplifiers and the vector modulators. These components can be optimized separately once the output and input characteristics of the reference arm have been decided. If manufacturers of vector modulators specify distortion or noise at the device output, then they become independent of the actual gain setting, which simplifies the analysis.

We now develop expressions for the interference,  $I_{SYS}$ , noise,  $N_{SYS}$ , and signal,  $S_{SYS}$ , at the receiver output.

#### A. Third-order Intermodulation Distortion at the Receiver

For simplicity we consider that both the primary and the reference antenna pick equal powered jamming signal, i.e.  $X_{PRI} = X_{REF} = X$ . At the cancellation point, the cancellation signal ( $x_2$ ) is subtracted from the jamming signal ( $x_1$ ) to give the resultant signal ( $x_3 = x_1 - x_2$ ).  $X_3$  is the power of the resultant signal. The study here considers that the cancellation system has converged and perfect cancellation is achieved at the cancellation point, i.e.  $X_1 = X_2$  and  $X_3 = 0$ . Hence, the GPA gain,

$$G_e = \frac{1-C}{C} \quad (1)$$

When  $X_3 = 0$  or significantly small, the receiver does not produce any third-order intermodulation distortion components, thus distortion components are only produced at the GPA. The third-order intermodulation distortion [4],  $D$ , produced at the GPA output is,

$$D = \frac{G_e^3 \cdot X^3}{OIP3_e^2} \quad (2)$$

Substituting for  $G_e$  from Equation (1), the third-order intermodulation distortion at the receiver output is given by,

$$I_{SYS} = \frac{G_{RX} X^3 (1-C)^3}{OIP3_e^2 C^2}. \quad (3)$$

#### B. Signal and Noise at the Receiver

As mentioned earlier the primary antenna is aimed at picking the desired receive signal, hence, the signal level at the receiver output is given by,

$$S_{SYS} = S(1-C)G_{RX} \quad (4)$$

The primary and the reference antenna noises are uncorrelated to one another. They are white noise and have a noise temperature of  $T_0$  (standard noise temperature, 290K). Thus the total noise at the receiver output is given by,

$$N_{SYS} = k \cdot B \cdot G_{RX} (T_{RX} + T_e C + T_0) \quad (5)$$

where  $k$  is the Boltzmann's constant ( $1.38 \times 10^{-23}$  J/K) and  $B$  is the signal bandwidth (Hz).

All of the above three equations are affected by the coupler coefficient,  $C$ . Both the signal,  $S_{SYS}$  and the interference  $I_{SYS}$  tend to zero as  $C \rightarrow 1$ . Surprisingly, the signal to interference ratio improves, but unfortunately this does not apply to the SINR which includes the effect of noise.

#### C. Signal to Interference and Noise Ratio

Combining Equations (3, 4 and 5), the signal to interference and noise ratio at the receiver is as follows,

$$SINR_{SYS} = \frac{S(1-C)}{\frac{X^3(1-C)^3}{OIP3_e^2 C^2} + k \cdot B \cdot (T_{RX} + T_e C + T_0)} \quad (6)$$

and is a function of the dynamic range of the reference path, the excess noise temperature of the receiver, the power of the jammer and coupler value. In the next section we determine the Coupler 1 value that gives the highest SINR.

### III. OPTIMUM COUPLING

For a certain strength of the jamming signal,  $X$ , we can optimize the coupler value  $C$  to give the largest possible SINR. We differentiate  $SINR_{SYS}$  with respect to  $C$ ,

$$\frac{dSINR_{SYS}}{dC} = \frac{S \cdot OIP3_e^2 \cdot C \cdot (2(1-C)^3 X^3 - k \cdot B \cdot OIP3_e^2 \cdot C^3 (T_0 + T_e + T_{RX}))}{(k \cdot B \cdot OIP3_e^2 \cdot C^2 (T_0 + C T_e + T_{RX}) + (1-C)^3 X^3)^2} \quad (7)$$

Setting  $\frac{dSINR_{SYS}}{dC} = 0$ , for  $0 < C < 1$  gives,

$$\frac{1-C}{C} = \sqrt[3]{\frac{k \cdot B \cdot OIP3_e^2 (T_0 + T_e + T_{RX})}{2X^3}} \quad (8)$$

which has one real root and two imaginary roots.  $C$  is a power gain and must be real, therefore there is only one extremum. Thus,

$$C_{opt} = \frac{2^{1/3} X}{Q^{1/3} + 2^{1/3} X} \quad (9)$$

where,

$$Q = k \cdot B \cdot OIP3_e^2 \cdot (T_0 + T_e + T_{RX}) \quad (10)$$

Inspecting Equation (6), we note that SINR is always positive, and has a value of 0 at both ends of  $C$ 's domain.

$$\begin{aligned} SINR_{SYS} &> 0 \\ C \rightarrow 0, SINR_{SYS} &\rightarrow 0 \\ C \rightarrow 1, SINR_{SYS} &\rightarrow 0 \end{aligned} \quad (11)$$

Hence,  $C_{opt}$  gives the maximum value of  $SINR_{SYS}$ .

From, Equation (9),  $C_{opt}$  is a function of  $X$  and  $Q$ .  $X$  is the power jamming signal. When  $X$  is large the third term starts dominating and  $C_{opt}$  asymptotes to 1, i.e.,  $C_{opt}(dB) \rightarrow 0$  in the log scale, as shown in Fig. 3. Further, using Taylor's series,

$$C_{opt} = \frac{2^{1/3}}{Q^{1/3}}X - \frac{2^{2/3}}{Q^{2/3}}X^2 + \frac{2}{Q}X^3 - \frac{2^{4/3}}{Q^{4/3}}X^4 + \dots \quad (12)$$

When  $X$  is small the first term in Equation (12) dominates and there is a linear relationship between  $X$  and  $C_{opt}$  with a slope of 1 in the log scale (i.e.  $C_{opt}(dB)$  is proportional to  $X(dB)$ ), as shown in figure,

$$C_{opt}(dB) = -\frac{1}{3}Q(dBW^3) + X(dB) + 1(dB) \quad (13)$$

$Q$  is a function of the dynamic range components ( $OIP3_e$  and  $T_e$ ) of the reference path and the noise figure ( $T_{RX}$ ) of the receiver;  $Q$  has a unit of Watts<sup>3</sup>. Note,  $Q$  is not dependent on  $IIP3_{RX}$ , since we assume perfect cancellation and therefore no jamming signal reaches the receiver. In the linear region increasing  $Q$  by 10dB decreases  $C_{opt}$  by  $3\frac{1}{3}$ dB. The value of  $Q$  characterizes the reference path and the sensitivity of the receiver. An increase in  $Q$  makes noise in the system more dominant; a 10dB increase in  $Q$  could either be a 10dB increase in noise,  $kB(T_0 + T_e + T_{RX})$ , or a 10dB increase in  $OIP3_e$ , which signifies a 10dB decrease in distortion Equation (2); in either case the noise to distortion ratio increases by 10dB. Vice versa, a decrease in  $Q$  makes distortion in the reference path more dominant.

The effect of the receiver noise figure is also covered in these equations. Receivers with low sensitivity (high  $T_{RX}$ ) will have a high  $Q$  value, implying a larger jamming signal for the same optimum coupler value. This is intuitively correct since a high effective noise floor allows higher distortion levels.

#### IV. HARDWARE SETUP AND CONVERGENCE

A two-tone test is carried out on the proposed cancellation system to further study the SINR characteristics of the system and verify our theory with practical results.

In order to have a controlled experiment that focuses on the actual SINR performance of the cancellation scheme, signals were all directly coupled into the system, no antennas were

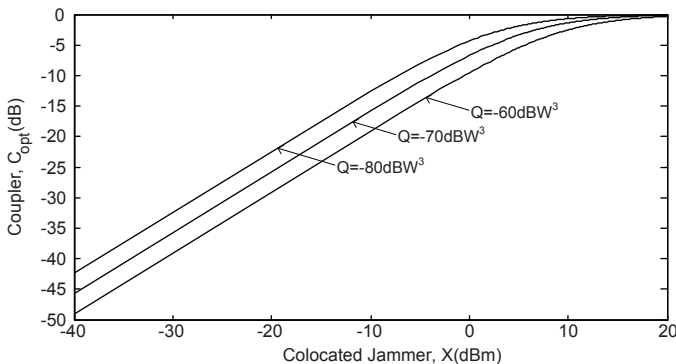


Fig. 3. Optimum Coupler,  $C_{opt}$ , as a function of the jammer,  $X$ , and the  $Q$  value ( $Q$  is primarily a function of the dynamic range of the components in the reference path).

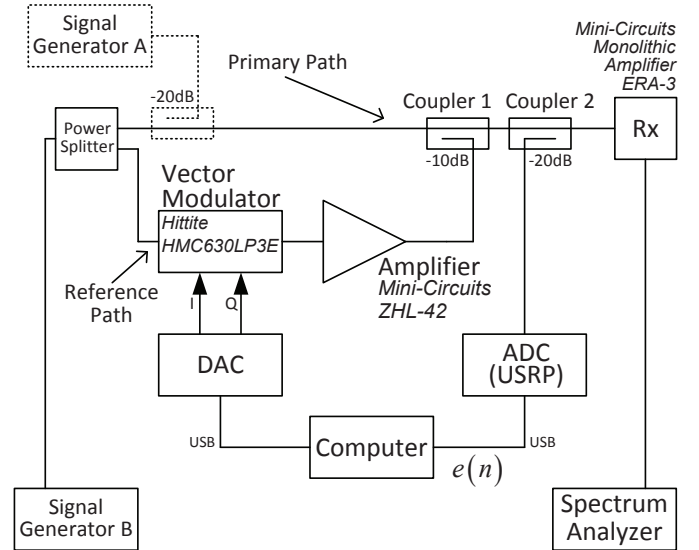


Fig. 4. Laboratory Setup: Signal Generator A generates the desired signal,  $S$ , and Signal Generator B generates the two tone jamming signal which is split into two with the Power Splitter to have equal levels of jammer,  $X$ , on both the Primary and the Reference Path.

used. Fig. 4 shows the two tone test setup of the proposed cancellation system. The gain-phase adjuster is realized with the use of a vector modulator [13] and an amplifier [14]. The vector modulator provides the required attenuation on the reference path when the jamming signal is larger than that of the primary. The amplifier provides the gain required to compensate for the coupler and the amplification required to eliminate the jammer in the primary path. An attenuator in front of the GPA might also be required if the copy of the jamming signal on the reference path is high.

The adaptive cancellation process works by learning the energy at the output of the cancellation and minimizing it. We use a  $-20$ dB coupler (Coupler 2) to couple out a sample from the cancellation output; a USRP is used to measure the sample in IQ components within a computer, then an algorithm evaluates the energy of the sample, the algorithm takes the energy as a cost function and minimizes it by iteratively changing the input voltage to the vector modulator using a DAC. The cost function is given by,

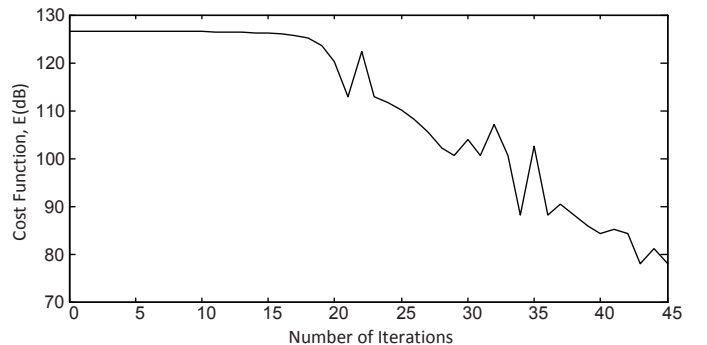


Fig. 5. Learning curve of the adaptive cancellation system during a two-tone test with an input power of  $-10$ dBm.

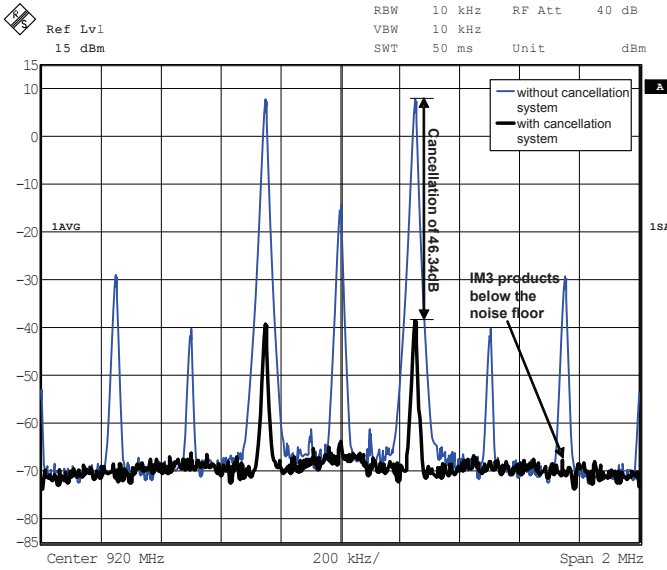


Fig. 6. Spectrum at the receiver with and without the proposed cancellation system during a two-tone test with an input power of -10dBm. The desired signal is not included.

$$CF = \sum_{n=1}^{1500} e_n \cdot e_n^* \quad (14)$$

where  $e(n)$  is a complex baseband sample from the USRP working as an ADC. If we assume the noise, signal and the distortion products are uncorrelated then,

$$CF = \left( \frac{\left( (1-C) + G_e C - 2\sqrt{G_e(1-C)C} \right) X}{+ \frac{S_{SYS} + I_{SYS}}{G_{RX}} + k \cdot B (T_e C + T_0)} \right) C_2 \quad (15)$$

where the coupling path gain of *Coupler 2*,  $C_2 = -20$ dB, and reaches a global minimum of,

$$CF_{min} = \left( \frac{S_{SYS} + I_{SYS}}{G_{RX}} + k \cdot B (T_e C + T_0) \right) C_2 \quad (16)$$

when Equation (1) applies.

The DAC has a resolution of 1mV, the algorithm iterates and minimises energy ( $CF$ ) in steps of 100mVs and then 10mVs and finally 1mV. Fig. 5 shows such a learning curve during a two-tone test. The cost function takes about 45 iterations to reach its minimum value. Each iteration takes  $187.5\mu s$  to obtain 1500 samples for the  $CF$  estimate at a USRP sample rate of 8M samples/s. The total convergence time is a respectable 8.4375ms.

Fig. 6 illustrates the spectrum at the receiver with and without the cancellation system. The IM3 products are reduced below the noise floor of the spectrum analyzer. The automated cancellation system achieves a cancellation of about 46dB, which is 7dB less than what was achieved with a manual cancellation system [11]. One of the causes is a large noise component,  $k \cdot B (T_e C + T_0) C_2$ , in the  $CF$  due to the wide bandwidth of the measuring system (in this case 8MHz). A wide-band receiver is needed in the feedback loop since the exact frequency of the jamming signal is unknown. An

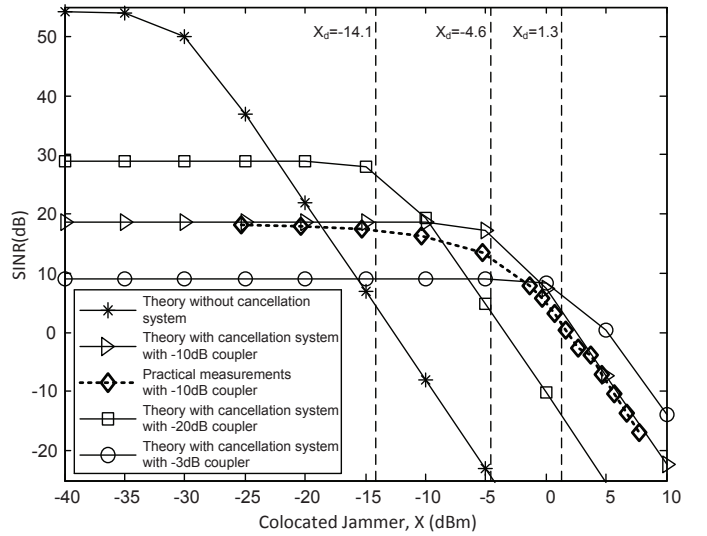


Fig. 7. SINR vs Jammer with Different Couplers. Noise bandwidth,  $B = 5$ MHz.

alternate solution using a frequency scanning narrowband receiver would also work.

## V. RESULTS

Fig. 7 compares the SINR of the receiver without the cancellation system (from hereon referred to as the ‘do-nothing’ system) to the receiver with the cancellation system over a range of co-located jammers from -40dBm to 10dBm. The theoretical calculations are based on a receiver with  $G_{RX} = 19$ dB, input IP3,  $IIP3_{RX} = 6$ dBm and a noise factor,  $F_{RX} = 2.7$ dB; these specifications align with the Mini-Circuits Monolithic Amplifier ERA-3 [15] that we use for our practical measurements. Similarly, for the  $OIP3_e$  value and the  $T_e$  value of the GPA we refer the combined specification values of the vector-modulator (Hittite HMC630LP3E) and amplifier (Mini-Circuits ZHL-42) to the amplifier output.

At low jamming levels the ‘do-nothing’ system has better SINR performance than the proposed cancellation system. This is because of additional noise from the reference path and the reduction in signal amplitude caused by the coupler. But at higher jamming levels increasing receiver distortion in the ‘do-nothing’ system causes its SINR to fall below that of the cancellation system. The cancellation system removes the jamming signal on the primary path before the receiver and hence there is no receiver distortion. The distortion in the system then depends on the combined IP3 properties of the components in the reference path. Eventually reference path distortion becomes dominant as  $X$  continues to increase and the cancellation system enters the waterfall region. The slope of all curves in the waterfall region are the same, so despite worsening SINR’s the canceling system always outperforms the ‘do-nothing’ system.

The coupler is a compromise between the noise and distortion introduced at the receiver. It determines the onset of the waterfall region. From Equation (9), the coupler optimizes the system for a design jamming level,  $X_d$ . Jamming levels lower than  $X_d$  generate negligible distortion and the SINR is

dominated by the noise term. The  $SINR_{SYS}$  value forms a plateau at,

$$SINR_{SYS}|_{plateau} = \frac{S(1-C)}{k.B(T_{RX} + T_e C + T_0)}. \quad (17)$$

As the jamming levels start getting larger, i.e.  $X > X_d$ , the distortion component dominates the SINR value,

$$SINR_{SYS}|_{waterfall} = S(1-C) \left/ \frac{X^3(1-C)^3}{OIP_3 e^2 C^2} \right. \quad (18)$$

and we have the waterfall region on the logarithmic graph with a slope of three.

Fig. 7 also compares the SINR performances with different coupler values. Consider the middle curve that is optimized for a jammer of  $X_d = -4.6\text{dBm}$  and uses a  $-10\text{dB}$  coupler (i.e.  $C = -10\text{dB}$ ). A higher coupling factor on *Coupler 1* requires less gain on the GPA for the cancellation. Hence, smaller distortions are produced for the same level of jammer. This is illustrated by the  $-3\text{dB}$  coupler line, optimized for  $X_d = 1.3\text{dBm}$ . Better SINR performance is obtained for  $X > 0\text{dBm}$ . But this performance enhancement comes at a price, higher coupling allows more noise from the reference path and hence the noise dominated plateaus are at lower SINR levels. The figure illustrates the plateau of the  $-3\text{dB}$  coupler at  $9\text{dB}$  SINR which is less than the plateau of the  $-10\text{dB}$  coupler at  $18.6\text{dB}$  SINR. Vice versa, a  $-20\text{dB}$  coupler that optimizes for  $X_d = -14.1\text{dBm}$  gives lower SINR performance than the  $-10\text{dB}$  coupler system for  $X > -10\text{dBm}$ ; and has a plateau at  $29\text{dB}$  SINR better than  $18.6\text{dB}$  SINR of the  $-10\text{dB}$  coupler.

SINR measurements were performed on the hardware tested to corroborate the analysis results. A  $-10\text{dB}$  cancellation coupler (*Coupler 1*) was used. The spectrum analyzer was used to measure the signal, noise and distortion components at the output of the receiver's LNA. The two tone jamming signal was generated, with powers ranging from  $-25\text{dBm}$  to  $8\text{dBm}$  to measure the IM3 products. The above were used to calculate the SINR and plotted against the input jamming signal levels,  $X$  as shown by the dotted line of Fig. 7. Our practical measurements fell slightly short of the theoretical results of the system; this is because of distortion products produced by the signal generator themselves and difficulties of measuring distortion levels close to the spectrum analyzer's own noise floor. These extra distortion products affect the result mostly in the transition region from a noise dominated plateau to a distortion dominated waterfall, where neither the noise or the distortion from our system is dominant. Apart from the transition region, the results agreed with the analysis in the plateau region and waterfall region to within  $1\text{dB}$ .

## VI. PRACTICAL ISSUES

A key issue in the practical realization of the technique is to resolve the most probable situation where the reference antenna picks up a copy of the desired signal ( $s_{ref}$ ) along with the copy of the jamming signal  $x_{ref}$ . This component ( $s_{ref}$ ) of the desired signal (shown dotted in Fig. 1) in the reference path may cause the cancellation of the desired signal ( $s$ ) at the receiver. As such, the scheme requires the signal to interference

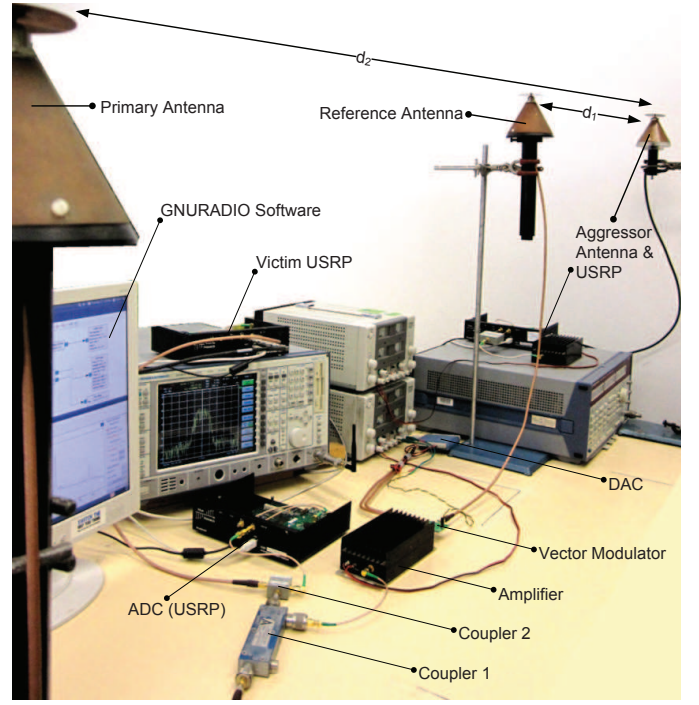


Fig. 8. Experimental Setup

ratio on the primary antenna ( $SIR_{PRI} = S/X_{PRI}$ ) to be adequately more than the signal to interference ratio on the reference antenna ( $SIR_{REF} = S_{REF}/X_{REF}$ ) to avoid any major cancellation of the desired signal.

At the receiver, after the reference path is scaled by the coefficient  $g$  and subtracted from primary path the received signal is,

$$r = x_{pri} - g.x_{ref} + s - g.s_{ref} \quad (19)$$

When  $g$  is scaled to remove the jamming signal components, then the received signal strength is given by,

$$r = s - g.s_{ref} : g = \frac{x_{pri}}{x_{ref}} \quad (20)$$

Now, if we have  $SIR_{PRI} > SIR_{REF}$  by a factor of  $M = m^2$ , i.e.,

$$\frac{SIR_{PRI}}{SIR_{REF}} = M \Rightarrow \frac{s}{x_{pri}} \left/ \frac{s_{ref}}{x_{ref}} \right. = m \quad (21)$$

which is further evaluated using Equation(20),

$$\frac{x_{pri}}{x_{ref}} = g = \frac{1}{m} \cdot \frac{s}{s_{ref}} \quad (22)$$

Thus, using Equation (22) the received signal is,

$$r = s \left( 1 - \frac{1}{m} \right) \quad (23)$$

The phase of  $m$  determines whether or not the received signal,  $r$ , is canceled or boosted. This phase is determined by the uncontrolled incoming components of the desired signal. The worst case phase angle  $\arg(m) = 0$  is assumed. The nulling of the jammer will not effect the received signal if  $M$ , the difference between the SIR's is large. This could be achieved by the use of a directly coupled signal from the aggressor's antenna feed cable, avoiding the need for a

reference antenna. Alternatively, if this is not practical, we take advantage of the fact that the desired signal is generally weak and far away from the base station, in which case its average signal strength will be the same on both the primary and the reference antennas. Therefore the SIRs can be changed by altering their distances to the aggressor antenna; normally, we decrease the SIR on the reference antenna by mounting it closer to the aggressor than the primary antenna. Alternatively, the reference antenna could be made directional and pointed at the aggressor. In the experiment of Fig. 8 we use omni-directional discone antennas and mount the reference antenna  $d_1 = 0.15$  meters from the aggressor, whereas the primary/victim antenna is mounted  $d_2 = 1.15$  meters from the aggressor to give an SIR ratio of  $M = (d_2/d_1)^2 = 59$  (based on the  $1/d^2$  path loss model). According to Equation (23), the worst case cancellation on the desired signal,  $S$ , is limited to a maximum value of  $-1.2$ dB. And in the best case the desired signal could gain  $+1.06$ dB.

Fig. 8 shows the over-the-air experimental setup. This is in accordance with the block diagram in Fig. 1. The transmitter and the receiver for the desired signal in the experiment are USRP units using GNU radio software. The co-located aggressor is also a USRP unit transmitting two large jamming signals with the help of an amplifier (Mini-Circuits ZHL-42). The cancellation loop on the reference path uses a  $-20$ dB coupler (*Coupler 1*) with  $13$ dB net amplification (Minicircuits ZX60-33LN+6dB attenuator) and the same Hittite vector modulator. The lower net amplification reduces cancellation loop noise, but is still high enough to cancel the jammers.

To demonstrate the performance of the system with modulated signals we use a narrow band ( $12.5$ kHz) QPSK modulated signal for both the desired and aggressor signals. The symbol rate is  $7.8125$ ksymbols/sec and filtered with a Nyquist filter with  $50\%$  excess bandwidth.

Fig. 9 shows the four constellation points of the received desired signal, along with a  $2$ MHz frequency spectrum centred at  $920$ MHz showing the jammers, the intermodulation products and the desired signal.

Fig. 9(a) shows three spectrum traces. Trace A (purple) at the bottom represents the noise floor with a  $50\Omega$  termination replacing the antenna at the primary input and the cancellation loop turned off (i.e. the components of the cancellation loop switched off adding zero noise to the overall system). The noise figure of the receiver without the cancellation loop is measured to be  $2.2$ dB. Trace B (red) in the middle represents the noise floor of the total system with the cancellation loop turned on and  $50\Omega$  terminations at the primary and reference antenna inputs. The noise figure of the receiver with the cancellation loop turned on is measured to be  $7.2$ dB. The increase of  $5$ dB in the receiver noise figure is due to the noise added by the components of the cancellation loop.

Trace C on the top (blue) shows reception from the primary antenna without any jammer and the cancellation circuit turned off. The low power transmitter for the desired signal is mounted in the next room and its spectrum is shown by the peak at  $920.75$ MHz (shown as an offset of  $0.75$ MHz on the figure, with  $0$  representing  $920$ MHz). The scatter plot on the left hand side shows the received QPSK constellations at a

signal to noise ratio of about  $26$ dB. The spur at  $920.27$ MHz is an unrelated external transmission. The spur in the middle is the LO leakage of the relatively inexpensive USRP receivers. A point to note is the overall radiated noise received in the  $900$ MHz ISM band dominates the receiver noise (Trace A) by about  $7$ dB. This noise floor will dilute the effect of a  $5$ dB rise in the receivers noise figure when the cancellation loop is activated.

The aggressor transmitter carries two equal power transmissions at  $919.75$ MHz and  $920.25$ MHz. These couple into the victim USRP receiver at an aggregate jamming strength of  $-36$ dBm; enough to generate intermodulation products including the two dominant components at the third order frequencies of  $919.25$ MHz and  $920.75$ MHz. The latter falls directly on to the channel of our desired signal and causes interference. Fig. 9(b) shows the constellations are unrecognizable as a result of the interference. The spectrum shows the jammers, the desired signal and the odd and even order intermodulation products. The desired signal is completely masked by the distortion products. Note, the integrity of the transmitted spectrum from the jammer was verified using a spectrum analyzer; no intermodulation products were produced by the jammer.

Fig. 9(c) illustrates the performance of the system with interference canceling switched on. The system canceled the jammers by a margin of  $25$ dB. Theoretically, this would be sufficient to reduce the third-order intermodulation products by  $75$ dB; well below the noise floor. The constellations are improved, but not to the extent of the original signal without interference. The constellation blooms are about  $4$ dB larger. A detailed investigation shows that the  $4$ dB rise in noise floor is partly due to the additional noise of the canceling loop ( $\approx 2.1$ dB) and partly to the noise transmitted from the jammers themselves. The latter can be fixed by better transmitter filtering (e.g. the duplexing filters and/or RF filtering before the final power amplifier stage).

As for the desired signal itself, its amplitude has hardly changed. In this instance  $m$  has a phase almost perpendicular to our desired signal causing a small cancellation of approximately  $0.3$ dB.

## VII. CONCLUSION

Co-location introduces undesired interference that produces distortion in the victim receiver. An adaptive cancellation system is used to overcome the interference and the performance improvement is optimized using an SINR analysis.

We confirmed that the choice of the cancellation coupler (*Coupler 1*) determines the balance between noise and distortion in the system. Furthermore, we proved there is a unique optimum coupler value ( $C_{opt}$ ) that optimizes the SINR for a given power of the jamming signal ( $X$ ). The expression for  $C_{opt}$  showed that at lower values of  $X$ ,  $C_{opt}$  is linear with  $X$  illustrated by a slope of  $1$  in the logarithmic scale (Fig. 3). The displacement of the line is set by  $Q$  which is a function of  $OIP3_e$  and  $T_e$  of the reference path and  $T_{RX}$  of the receiver. Higher  $Q$  values represent noise being more prevalent in the system than distortion, and permits a larger jamming signal for

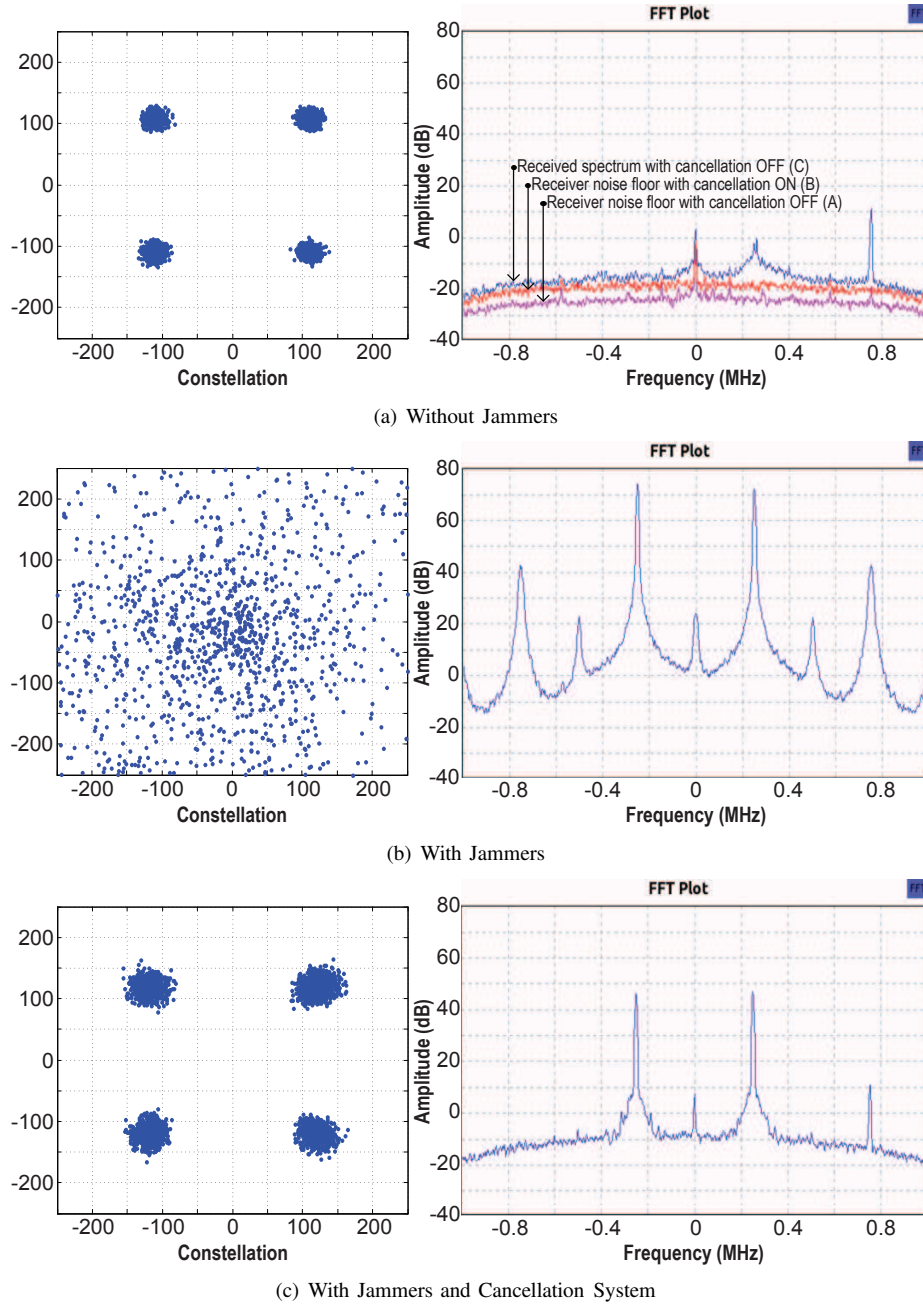


Fig. 9. Experiment Results. Signal constellation scatter plots (LHS) and GNU Radio spectrum plots (RHS). The GNU Radio spectrum plots show relative scales with 75dB representing  $-39\text{dBm}$ , and on the frequency scale 0 representing 920MHz.

the same optimum coupler. These equations can be used for choosing the reference path components to achieve a certain desired design performance of the scheme.

Jammers below the design jamming level,  $X_d$  (optimized by a certain coupler value), generate negligible distortion and the SINR graph forms a plateau. For jammers above  $X_d$ , distortion components dominate and we have the waterfall region in the SINR graph. We have developed expressions for the plateau and waterfall regions. We note that in the plateau region, the SINR is dominated by noise from the reference path and at low signals this leads to a degradation in performance compared to the ‘do-nothing’ scheme. It should be possible to identify this situation by measuring the energy on the reference antenna. In

the absence of any jammer we can turn OFF the cancellation path and revert back to the original sensitivity of the receiver; minus the small  $1 - C$  insertion loss of *Coupler 1* ( $\approx 0.5\text{dB}$  for a  $-10\text{dB}$  coupler).

The controlled experiment prototype using a  $-10\text{dB}$  cancellation coupler (*Coupler 1*) gave improved SINR (compared to the basic ‘do-nothing’ system) for jamming signals  $X > -18\text{dB}$  (Fig 7). The scheme achieved a significant 42dB SINR at the designed jamming level of  $X_d = -4.6\text{dBm}$ . In the waterfall region where  $X > X_d$ , the improvement was 45dB, which means that the tolerated jamming signal can be 15dB larger compared to the basic ‘do-nothing’ system with the same SINR. The SINR results agreed with the theoretical

predictions. Further, the over-the-air problem of signal self-cancellation can be controlled by proper placement of the reference antenna.

The system was made adaptive by reducing the energy at the cancellation output. A simple energy (diode) detector could be used for this purpose. The automated cancellation system is reasonably fast requiring a total of 8.4375ms (about 45 iterations) to converge; it reduced the jamming signal by 46dB (controlled experiment) and 25dB (over-the-air experiment); more than enough to suppress the IM3s. If faster convergence is necessary, then it should be possible to borrow algorithms from the extensive signal processing literature on null steering, phased array antennas, direction of arrival estimation and acoustic noise canceling [16] [17] [18].

An over-the-air demonstration in the 900MHz ISM band showed a 25dB reduction in jammer power and the elimination of all distortion products. The trade-off was a 5dB increase in receiver noise figure. In a quiet site, this directly transforms into a loss of receiver sensitivity. However sites that operate in an interference limited mode (urban cellular sites or ISM sites for example) will be degraded less by the loss in noise figure.

The paper establishes that a significant SINR performance enhancement can be achieved using a reference antenna based adaptive cancellation system.

## REFERENCES

- [1] F. German, K. Annamalai, M. Young, M. C. Miller, "Simulation and Data Management for Cosite Interference Prediction," in *Proc. IEEE International Symposium on Electromagnetic Compatibility*, July 2010.
- [2] I. Demirkiran, D. D. Weiner, A. Drozd and I. Kasperovich, "Knowledge-based Approach to Interference Mitigation for EMC of Transceivers on Unmanned Aircraft," in *Proc. IEEE International Symposium on Electromagnetic Compatibility*, July 2010.
- [3] J. J. Gavan and M. B. Shulman, "Effects of Desensitization on Mobile Radio System Performance, Part I: Quantitative Analysis," *IEEE Transactions on Vehicular Technology*, vol. VT-33, no. 4, pp. 285-290, November 1984.
- [4] B. Razavi, *RF Microelectronics*, Upper Saddle River, NJ: Prentice Hall, 1998.
- [5] B. Razavi, "Design Considerations for Direct-Conversion Receivers," *IEEE Transactions on Circuit and Systems II: Analog and Digital Signal Processing*, vol. 44, no. 6, June 1997.
- [6] W. Guthrie and D. Hanson. (2005, June 13). Co-Location Interference Mitigation. *White Paper*. Netcom Inc., USA. <http://www.netcominc.com>
- [7] Alain Roussel, Charles W. T. Nicholls, and Jim S. Wight, "Frequency Agile RF Feedforward Noise Cancellation System," in *Proc. IEEE Radio and Wireless Symposium*, 2008.
- [8] S. Kannangara and M. Faulkner, "Analysis of an Adaptive Wideband Duplexer With Double-Loop Cancellation," *IEEE Transactions on Vehicular Technology*, vol. 56, issue 4, July 2007.
- [9] A. Raghavan, E. Gebara, E. M. Tentzeris and J. Laskar, "Analysis and Design of an Interference Canceller for Collocated Radios," *IEEE Transactions on Microwave Theory and Techniques*, vol. 53, no. 11, November 2005.
- [10] B. Widrow, J. R. Glover, J. M. McCool, J. Kaunitz, C. S. Williams, R. H. Hearn, J. R. Zeidler, E. Dong, Jr., and R. C. Goodlin, "Adaptive noise canceling: Principles and applications," *Proc. IEEE*, vol. 63, pp. 1692-1716, 1975.
- [11] S. Ahmed and M. Faulkner, "An Adaptive Cancellation System for a Co-Located Receiver and its Dynamic Range," in *Proc. IEEE Radio and Wireless Symposium*, January 2011.
- [12] Ettus Research LLC. Universal Software Radio Peripheral. *Data Sheet*. [Online]. Available: [http://www.ettus.com/downloads/ettus\\_ds\\_usrp\\_v7.pdf](http://www.ettus.com/downloads/ettus_ds_usrp_v7.pdf)
- [13] Hittite Microwave Corporation. HMC630LP3E Vector Modulator. *Data Sheet*. [Online]. Available: [http://www.hittite.com/content/documents/data\\_sheet/hmc630lp3.pdf](http://www.hittite.com/content/documents/data_sheet/hmc630lp3.pdf)
- [14] Mini-Circuits. ZHL-42 Amplifier. *Data Sheet*. [Online]. Available: <http://www.minicircuits.com/pdfs/ZHL-42.pdf>
- [15] Mini-Circuits. Monolithic Amplifier ERA-3. *Data Sheet*. [Online]. Available: <http://www.minicircuits.com/pdfs/ERA-3+.pdf>
- [16] L. C. Godara, "Application of Antenna Arrays to Mobile Communications, Part II: Beam-Forming and Direction-of-Arrival Considerations," in *Proceedings of the IEEE*, vol. 85, issue 8, pp. 1195-1245, August 1997.
- [17] H. Krim and M. Viberg, "Two Decades of Array Signal Processing Research: The Parametric Approach," *IEEE Signal Processing Magazine*, vol. 13, issue 4, pp. 67-94, July 1996.
- [18] S. M. Kuo and D. R. Morgan, "Active Noise Control: A Tutorial Review," in *Proceedings of the IEEE*, vol. 87, issue 6, pp. 943-973, June 1999.



**Shabbir Ahmed** graduated in Computer Science from North South University, Bangladesh in 2005. Following his graduation, he worked as an engineer in the telecommunication industry in Bangladesh for two and half years. He has experience in laying out fibre-optic links, deploying base stations and working with network switching subsystems. Shabbir joined the Centre for Telecommunication and Microelectronics at Victoria University in April 2008 for his Ph.D. He is among the few who has got the EAL Postgraduate Student Mobility Scholarship Program in Australia. His Ph.D. research investigates the major causes of interference that arise in colocating base station transceivers. His research interests are in software radios and RF systems.



**Mike Faulkner** received a B.Sc.(Eng) from London University, UK, and a Ph.D. from the University of Technology, Sydney, Australia. He is Professor at Victoria University, Melbourne, Australia. He founded and led the Mobile Communications and Signal Processing Research (MCSP) group in 1988 which morphed into Centre for Telecommunications and Micro-Electronics (CTME) in 2002. Prof. Faulkner has been involved in standardization and commercialization activities in the IEEE802.11n (WLAN) space. He currently leads the telecom and microelectronics group at the CTME. He has supervised research projects in radio propagation measurements (wideband channel sounding, direction of arrival etc.), MIMO, transceiver algorithms, architectures and circuits, physical layer signal processing, and modulation. His research interests cover all areas of wireless system design and his current activities are focused on cognitive radio and flexible transceiver designs.